Heliyon 9 (2023) e18774

Contents lists available at ScienceDirect

Heliyon

journal homepage: www.cell.com/heliyon

Transposon delivery for CRISPR-based loss-of-function screen in mice identifies NF2 as a cooperating gene involved with the canonical WNT signaling molecular class of hepatocellular carcinoma

Vincent W. Keng [a,b,*], Amy P. Chiu [b], Jeffrey C. To [a,b], Xiao-Xiao Li [a], Michael A. Linden [c], Khalid Amin [c], Branden S. Moriarity [d], Kosuke Yusa [e,f,**]

[a] The Hong Kong Polytechnic University Shenzhen Research Institute, Shenzhen 518057, China
[b] Department of Applied Biology and Chemical Technology, State Key Laboratory of Chemical Biology and Drug Discovery, The Hong Kong Polytechnic University, Kowloon, Hong Kong, China
[c] Department of Laboratory Medicine and Pathology, University of Minnesota, Minneapolis, MN 55455, USA
[d] Masonic Cancer Center, Department of Pediatrics, and Center for Genome Engineering, University of Minnesota, Minneapolis, MN 55455, USA
[e] Stem Cell Genetics, Institute for Life and Medical Sciences, Kyoto University, Kyoto, Japan
[f] Wellcome Sanger Institute, Cambridge CB10 1SA, UK

ARTICLE INFO

Keywords:
Hepatocellular carcinoma
Transposable elements
CRISPR/Cas9
CTNNB1
NF2

ABSTRACT

Various molecular subclasses of hepatocellular carcinoma (HCC) exists, with many novel cooperating oncogenes and tumor suppressor genes involved in its tumorigenesis. The emerging importance of WNT signaling in HCC has been established. However, the intricate genetic mechanisms involved in this complex signaling pathway remains to be elucidated. Importantly, while some cooperating genes have been identified, there are still many unknown genes associated with catenin beta 1 (*CTNNB1*)-induced HCC. Mutations in both oncogenes and tumor suppressor genes are required for HCC tumorigenesis. The emergence of the CRISPR/Cas9 system has allowed researchers now to target both alleles efficiently. In this novel study, the Sleeping Beauty transposon system was used as a gene delivery system *in vivo* to stably integrate an expression cassette that carry pools of gRNAs and overexpress a mutant version of *CTNNB1* into the hepatocyte genome. We identified 206 candidate genes that drive HCC tumorigenesis in the context of WNT signaling activation and, neurofibromin 2 (*NF2*) gene, a known tumor suppressor gene with clinical relevance was validated in this proof-of-principle study.

1. Introduction

Hepatocellular carcinoma (HCC) is amongst the top leading cause of cancer-related death globally (affecting over 700,000 patients per year) and the incidence of this deadly disease is increasing [1]. The development of HCC is a very serious malignancy, which is

* Corresponding author. Department of Applied Biology and Chemical Technology, State Key Laboratory of Chemical Biology and Drug Discovery, The Hong Kong Polytechnic University, Kowloon, Hong Kong, China.
** Corresponding author. Stem Cell Genetics, Institute for Life and Medical Sciences, Kyoto University, Kyoto, Japan.
E-mail addresses: vincent.keng@polyu.edu.hk (V.W. Keng), k.yusa@infront.kyoto-u.ac.jp (K. Yusa).

https://doi.org/10.1016/j.heliyon.2023.e18774
Received 6 July 2023; Received in revised form 25 July 2023; Accepted 27 July 2023
Available online 28 July 2023

typically diagnosed at a late stage and carries a very poor prognosis [2]. There are many associated risk factors of HCC: aflatoxins, chronic hepatitis caused by hepatitis viruses and alcohol abuse, obesity and other environmental factors can contribute to the onset of HCC [3]. However, the genetic mechanism(s) associated with these associated risk factors remain elusive. Differences in disease incidence rates reflect the regional diversity that is mostly related to geographic distribution of viral hepatitis, the major contributing factor of HCC [2]. Gender also influences risk of the disease with males showing a higher increase in prevalence over females, with molecular data that explains this gender discrepancy [4–6]. It is clear that HCC is a very heterogeneous disease and many different molecular classes exists, depending on the gene expression profile and gene copy number changes [7,8]. One particular molecular class-of-interest and subject of this study is the WNT signaling-associated subgroup, which often have mutations in the catenin beta 1 (*CTNNB1*) gene, and which are identified in ~40% of all human HCCs [7,8]. We have previously shown that this oncogene can rapidly cause HCC *in vivo* in a non-gender bias manner [5]. Like in many other different cancers, tumor suppressor genes are likely to play a huge role in HCC tumorigenesis. Tumor protein p53 (*TP53*) mutations are frequently detected in HCC patients [9], while phosphatase and tensin homolog deficiency in mice results in steatosis and HCC [10]. However, it is clear that combinatory mutations in both oncogenes and tumor suppressor genes are equally important for HCC tumorigenesis. To date, many HCCs have no known drivers or with only one driver identified. While some studies have demonstrated the many subgroups of HCC exist, the complete understanding to the genetic mechanisms of these subgroups are still in its infancy.

Powerful technologies for forward genetic screens in mice, such as Sleeping Beauty (*SB*) transposon-mediated transposon mutagenesis, permit the simultaneous and unbiased identification of large sets of mutated genes in individual mouse cancers. The *SB* insertional mutagenesis screen has been successful in identifying many potential oncogenes and tumor suppressor genes responsible for HCC [5,11–17]. Therefore, these forward genetic screens have provided valuable insight into the molecular mechanisms associated with HCC and its metastatic process [11,12]. In addition, valuable genetic information obtained from these screens will provide new targets for therapy and appropriate molecular-based staging systems. However, the caveat of using *SB* technology for recessive or loss-of-function screen is that both alleles have to be mutated in order for complete tumor suppressor gene inactivation. In the forward genetic screens aforementioned, tumor suppressor genes identified usually have one allele mutated by the *SB* mutagenic transposon, while the other allele was probably inactivated by *de novo* mutation. Targeting one tumor suppressor gene allele inactivation may trigger cooperative events in tumorigenesis. Usually, a predisposed genetic background, like *MYC*-expression, is required to identify tumor suppression genes in *SB* forward genetic screens [13].

Clustered, regularly interspaced, short palindromic repeat (CRISPR)-Cas system has been recently shown to be an effective mammalian genome editing system [18–23]. In this study, the *SB* transposon system was used as a gene delivery system *in vivo* to stably integrate an expression cassette that carry pools of gRNAs and overexpress a mutant version of *CTNNB1* into the hepatocyte genome. Due to the novel animal model system that can select and enrich for stable events, hepatocytes that have a selective growth advantage as a result of the introduced transgenes (namely *CTNNB1* and gRNAs) would proliferate and result in tumorigenesis. Therefore, the combination of the *SB* transposon and the CRISPR-Cas9 systems will allow for a powerful genome wide loss-of-function screen to discover genes and pathways that drive HCC tumorigenesis in the context of WNT signaling activation. Using a gRNA hit frequency rate criterion, 206 genes were identified in the *in vivo* forward genetic screen. From these 206 genes, neurofibromin 2 (*NF2*) gene, a known tumor suppressor gene with clinical relevance was validated in this proof-of-principle study.

NF2, or merlin, belongs to the ezrin-radixin-moesin (ERM) protein family and its dysregulation has been associated with different types of sporadic carcinomas such as neurofibromatosis type II [24]. *NF2* is an established tumor suppressor gene involved in multiple cancers: such as mesothelioma, bladder cancer, breast cancer, glioblastoma, osteoblastoma, thyroid cancer, craniopharyngioma and pancreatic cancer [25–32]. Many studies have elucidated the genetic mechanisms for inducing tumorigenesis as the result of NF2 inactivation, such as activation of YAP/TAZ transcriptional factor, promoting cell proliferation, invasion and stemness [25,33]. Disruption of NF2 and the involvement of the Hippo signaling pathway in hepatic progenitor cells may lead to the development of HCC [34]. While the cross-talk between Hippo and WNT signaling in HCC has been established, this study demonstrates the novel genetic association between *NF2* and *CTNNB1* in HCC tumorigenesis.

2. Materials and methods

2.1. Transgenic mice

All animals were housed at the Centralised Animal Facility (CAF), received humane care and the ethics approval number 17-18/34-ABCT-R-GRF has been approved by the Animal Subjects Ethic Sub-Committee (ASESC) – both CAF and ASESC are research units of The Hong Kong Polytechnic University (HKPU), Hong Kong, China. Two different strains of transgenic mice were utilized in this study: (1) Fumarylacetoacetate hydrolase (*Fah*)-deficient mice (mixed genetic background C57BL/6 × 129/Sv) carrying the ubiquitously expressing Sleeping Beauty (*SB*) transposase transgene knocked into the *Rosa26* locus (*Rosa26*-SB11) – known as *Fah*/SB11 (FS) mice; and (2) *Fah*-deficient mice (mixed genetic background C57BL/6 × 129/Sv) carrying the Cas9 transgene knocked into the *Rosa26* locus (*Rosa26*-EC1N) – known as *Fah*/EC1N mice (EC1N mice were obtained from Wellcome Sanger Institute, United Kingdom) [35]. Both transgenic strains were maintained separately on 7.5 μg/mL nitisinone or NTBC (Swedish Orphan Biovitrum) supplemented drinking-water [36]. When required for the introduction of the *CTNNB1*/gRNA library by hydrodynamic injection, both transgenic strains were bred together to obtain the experimental *Fah*/SB11/EC1N (FSE) mice. The FS transgenic mouse strain was used for the hydrodynamic injection of transposon plasmids that do not require Cas9 recombinase activity.

2.2. Guide RNA (gRNA) library

Using the MGI Gene Expression Database, 3351 protein-encoding genes were identified to be expressed in the mouse adult liver. We then synthesized 16,705 gRNAs (CustomArray Inc., USA) to target these mouse hepatocyte-specific genes and cloned them into a *SB* transposon-based vector to stably express these gRNAs in the livers of FSE mice. On average, 5 gRNAs were designed to target each mouse liver protein-encoding gene (Supplementary Data 1). One hundred and eighty-six gRNAs (targeting 73 genes) were excluded from counting but were still injected as part of the gRNA library into FSE mice. The transposon vector carries the gRNA-expressing cassette and a human EF1a promoter-driven cassette carrying a T2A-linked ORF of *GFP*, *Fah* to rescue the *Fah*-deficient hepatocytes, and the constitutively active *CTNNB1*-S33Y (*CTNNB1*^{S33Y}) (Fig. 1A). The construction of the transposon vector carrying the *CTNNB1*^{S33Y} oncogene alone has been previously described (Fig. 1A) [5]. The pT2/GD-IRES-GFP-CTNNB1 transposon vector was hydrodynamically injected into FS mice.

2.3. Hydrodynamic tail vein injection

Transposon expression vectors (20 μg per vector) were introduced into the livers of 45-day old FSE or FS mice by hydrodynamic tail vein injection [37–40]. As the CTNNB1 molecular subclass of HCC is not associated with gender bias, both male and female mice were utilized in this study [5,41]. NTBC supplemented water was immediately replaced with normal drinking water after injection. The mice were sacrificed between 17- to 113-days post-hydrodynamic injection (PHI) and livers isolated for further analyses. Liver tumor nodules and adjacent normal tissues from 65- to 113-days PHI were used for next-generation sequencing (NGS).

2.4. Liver tumor analyses

The entire mouse liver was harvested, weighed and rinsed with cold phosphate buffered saline (PBS). Tumor nodules were counted, isolated and separated for total RNA and genomic DNA extraction. Samples for RNA extraction were stored in RNAlater Stabilization solution (Life Technologies) at −80 °C. RNA isolation was done using Trizol reagent (Life Technologies) according to the manufacturer's protocol. Genomic DNA was isolated using standard proteinase-K treatment, phenol-chloroform extraction and ethanol precipitation. Genomic DNA was then dissolved in sterile TE (10 mM Tris-HCl (pH 7.5), 1 mM EDTA (pH 8)) and quantified using a Nanodrop spectrophotometer. Histological sections were only taken for larger tumor nodules (>2 mm in diameter). Formalin fixed-paraffin embedded sections from various tissues were sectioned at 5 μm using a standard microtome (Leica), mounted and heat-fixed onto glass slides. Tissue section slides were either processed and stained with hematoxylin-eosin (HE) using standard protocols. Histopathological analyses were performed in part by board-certified human pathologists (M.A.L. and K.A.).

2.5. RT-PCR

First strand cDNA synthesis was performed using PrimeScript RT Master Mix (Takara) as described by the manufacturer using 1 μg total RNA as template. Both reactions with (RT+) and without (RT-) the reverse transcriptase were performed for all the samples. Subsequent PCR was performed using 1 μL of the cDNA as template with various primer pairs. Primer sequences for alpha-fetoprotein (*Afp*) were forward 5′-CCTGTGAACTCTGGTATCAG-3′ and reverse 5′-GCTCACACCAAAGCGTCAAC-3' (amplicon 410 bp); *Cas9* forward 5′-TGGGAAATACAGACCGCCAC-3′ and reverse 5′-AGCTGTCCGTTTGAGACGAG-3' (amplicon 101 bp); constitutively active catenin beta 1 S33Y (*CTNNB1*) forward 5′-GCCGCTTACTTGTCATCGTCGTCCT-3′ and reverse 5′-TGTTCCGAATGTCTGAGGACAAGCC-3' (amplicon 400 bp); fumarylacetoacetate hydrolase (*Fah*) forward 5′-ATGAGCTTTATTCCAGTGGCC-3′ and reverse 5′-ACCA-CAATGGAGGAAGCTCG-3' (amplicon 503 bp); green fluorescent protein (*GFP*) forward 5′-ACTTGTACAGCTCGTCCATGC-3′ and reverse 5′-TCGTGACCACCCTGACCTAC-3' (amplicon 537 bp); Sleeping Beauty transposase (*SB11*) forward 5′-ATGGGAAAAT-CAAAAGAAATCAGCC-3′ and reverse 5′-CGCACCAAAGTACGTTCATCTCTA-3' (amplicon 221 bp); actin beta (*Actb*) forward 5′-GTGACGAGGCCCAGAGCAAGAG-3′ and reverse 5′-AGGGGCCGGACTCATCGTACTC-3' (amplicon 938 bp). PCR conditions were 25–30 cycles to avoid amplicon saturation. Semi-quantitative analyses of non-saturated RT-PCR amplicons were performed using the ImageJ 1.40J software (NIH, Maryland, USA). Briefly, intensity of non-saturated RT-PCR amplicon bands was measured as an arbitrary value relative to *Actb* expression levels using ImageJ software.

2.6. Illumina sequencing of gRNAs

The procedure for sample preparation for Illumina sequencing of gRNAs has been previously published [18]. Briefly, the sequencing of all gRNAs in the genome-wide library involved PCR amplification of the region containing the gRNA using primers: gLibrary-HiSeq_50bp-SE-U1, 5′-ACACTCTTTCCCTACACGACGCTCTTCCGATCTCTTGTGGAAAGGACGAAACA-3′ and gLibrary-HiSeq_50bp-SE-L5, 5′-TCGGCATTCCTGCTGAACCGCTCTTCCGATCTTACCTTCGCCTCTCAATCAGC-3′ with Q5 Hot Start High-Fidelity 2X Master Mix (New England Biolabs, USA) using conditions recommended by the manufacturer. Two hundred picograms of the purified 1st PCR products was used for PCR enrichment with KAPA HiFi HotStart ReadyMix with the following conditions: 98 °C for 30 s, 12 cycles of 98 °C for 10 s, 66 °C for 15 s and 72 °C for 20 s, and the final extension, 72 °C for 5 min. The PCR products were purified with Agencourt AMPure XP beads in a PCR-product-to-bead ratio of 1:0.7. The purified libraries were quantified and sequenced on Illumina HiSeq2500 by 19-bp single-end sequencing. gRNA sequences were used to count the number of reads of each gRNA in the library.

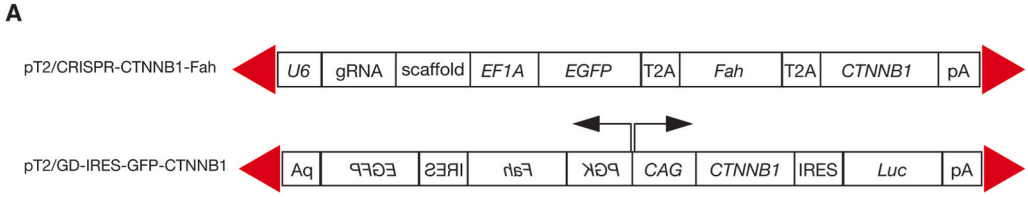

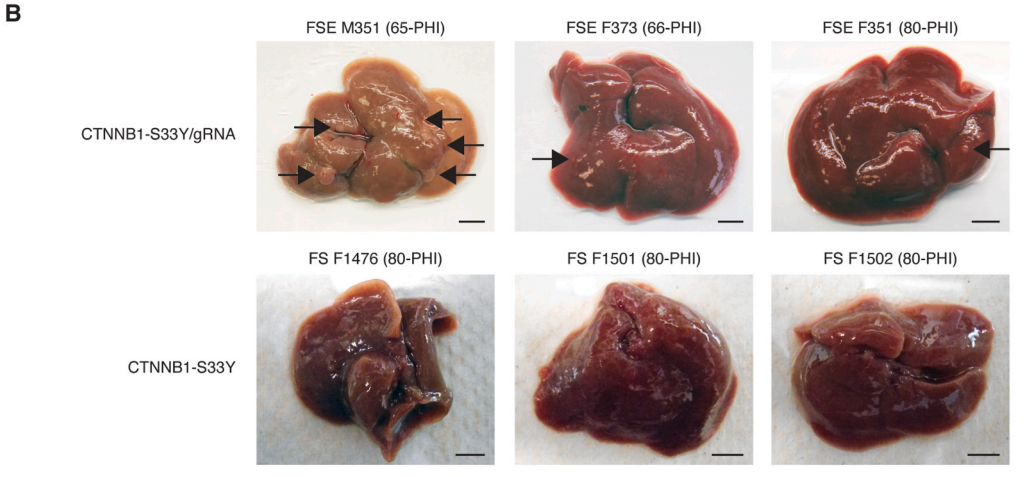

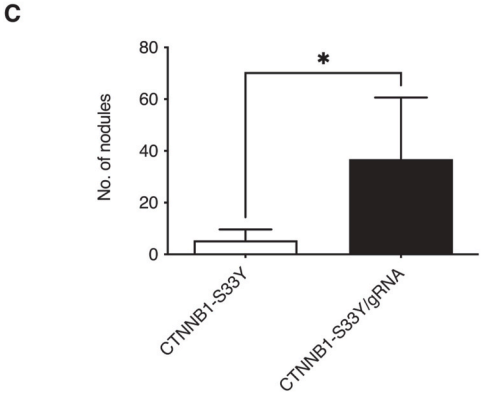

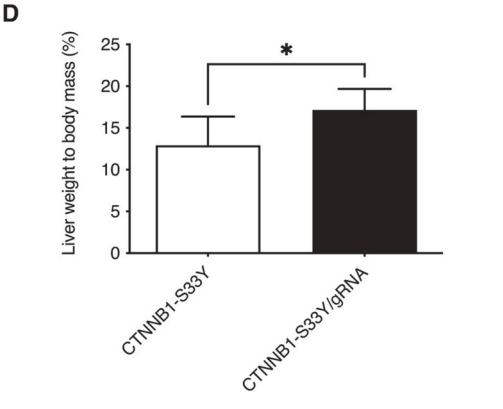

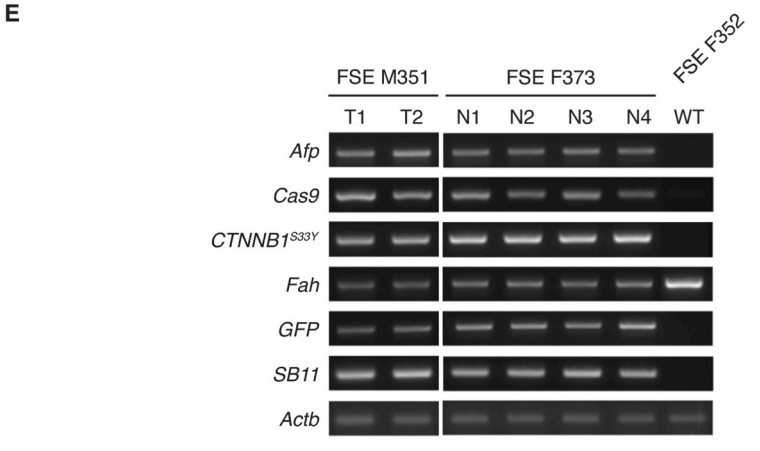

(caption on next page)

Fig. 1. *In vivo* transposon delivery system CRISPR-based screen for cooperating genes with *CTNNB1*-associated liver cancer tumorigenesis. (**A**) Representative transposon-based gene delivery vector for the pooled guide RNA and *CTNNB1*-overexpression (**top**) and bi-directional gene delivery vector for *CTNNB1*-overexpression only (**bottom**) for hydrodynamic tail vein injection. U6, U6 promoter; 20-bp guide sequence, 20-bp guide RNA (gRNA) sequence for specific gene; gRNA scaffold, sequence necessary for Cas9 binding; *EF1A*, elongation factor 1-alpha gene promoter; *EGFP*, enhanced green fluorescent protein reporter gene; *CTNNB1*, constitutively active catenin beta 1 gene with S33Y mutation; T2A, T2A peptide for ribosomal skipping; IRES, internal ribosome entry site; *Fah*, fumarylacetoacetate hydrolase gene; pA, polyadenylation tail; Flanking red arrowheads, inverted-repeat and direct-repeat recognition sequences for Sleeping Beauty transposase enzyme. (**B**) Representative photos of increased liver tumor burden in experimental animals co-injected with gRNAs and *CTNNB1* (**top panel**) compared with animals injected with *CTNNB1* alone (**bottom panel**). Arrows, tumor nodules; PHI, days post-hydrodynamic injection; scale bars, 0.5 cm. (**C**) Increased liver tumor burden in experimental mice co-injected with pooled gRNA library and *CTNNB1* ($n = 8$) compared with animals injected with *CTNNB1* alone ($n = 5$). *, $P < 0.05$ (unpaired Student *t*-test). (**D**) Statistically significant differences in liver to whole body weight percentage was observed between experimental mice co-injected with pooled gRNA library and *CTNNB1* ($n = 8$) compared with animals injected with *CTNNB1* alone ($n = 5$). *, $P < 0.05$ (unpaired Student *t*-test). (**E**) Representative RT-PCR analyses of liver samples taken from *Fah*/SB11/EC1N (FSE) mice injected with gRNAs together with $CTNNB1^{S33Y}$ expressing our transgene(s)-of-interest. T, liver tumor; N, macroscopically normal liver; WT, wild-type mouse liver. RT-negative controls did not show any detectable bands (*data not shown*). (For interpretation of the references to colour in this figure legend, the reader is referred to the Web version of this article.)

2.7. Cell culture

SNU449 is from the Human Liver Cancer Panel (ATCC® TCP-1011™) purchased from American Type Culture Collection (ATCC). Human hepatocyte line 7 (HHL7) is an immortalized human liver cell line [42]. SNU449 cells were cultured and maintained in RPMI 1640 medium with 10% fetal bovine serum (FBS) and 1% antibiotic-antimycotic (AA) at 37 °C under 5% CO_2 conditions. HHL7 cells were cultured and maintained in DMEM with 10% FBS and 1% AA at 37 °C under 5% CO_2 conditions. All cell culture media and supplements were purchased from Thermo Fisher Scientific.

2.8. CRISPR/Cas9 system gRNA design and plasmid construction

The CRISPR/Cas9 system was used to knockout *NF2* in HHL7 and SNU449 cell lines. gRNAs were designed and used as a pair to target specific domains of each gene to generate indels (Supplementary Table 1). The forward and reverse oligos of each gRNA were initially annealed together before ligating into the *Bbs*I site of pSpCas9(BB)-2A-Puro (PX459) V2.0, a gift from Dr Feng Zhang (Addgene plasmid #62988; http://n2t.net/addgene:62988; RRID:Addgeen_62988) as previously described [43]. The same process was used to construct the scramble gRNA control vector.

For each transfection reaction, 3 μg of each knockout vector was pooled and transfected into 1.5×10^5 cells in 6-well plates by ViaFect transfection reagent (Promega) according to the manufacturer's instruction. The same amount of scramble vector was used as a negative control. After 24 h post-transfection, cells were selected under 0.4 μg/mL of puromycin in medium for 5 days to select for successfully targeted pools. Pure single clones were selected from the transfected pool by single-cell dilution method – diluting to 50 cells/10 mL and plating out 100 μL/well in a 96-well plate. Successfully generated single clones were expanded into cell strains and used for different genetic analyses. Genomic DNA, RNA and protein were extracted using standard protocols.

2.9. qPCR analyses

Five hundred nanograms of total RNA from HCC cells and tissue samples was used as template for cDNA synthesis using PrimeScript RT Master Mix (Takara). Diluted cDNA (1:10 dilution) was mixed with SYBR Green Master Mix (Takara) and target primer sets, according to manufacturer's protocol. Target mRNA expressions were then determined by QuantStudio 7 Flex Real-Time PCR System (Thermo Fisher) (University Research Facility in Life Sciences of The Hong Kong Polytechnic University) using the following conditions: 1 cycle of 95 °C for 30 s, 40 cycles of 95 °C for 3 s and 60 °C for 30 s. Results were analyzed by the ΔΔCT method. The following primer sets were used: *NF2* forward 5′-TGCGAGATGAAGTGGAAAGG-3′ and reverse 5′-GCCAAGAAGTGAAAGGTGAC-3'; *ACTB* forward 5′-GCCGTCTTCCCCTCCATCGT-3′ and reverse 5′-TGCTCTGGGCCTCGTCGC-3'; *CTNNB1* forward 5′-AAAGCGGCTGTTCGTCACTGG-3′ and reverse 5′-CGAGTCATTGCATACTGTCCAT-3'; *MYC* forward 5′-CGGAAGGACTATCCTGCTGC-3′ and reverse 5′-CAAGACGTTGTGTGTTCGCC-3'; endoglin (*ENG*) forward 5′-CGGTGGTCAATATCCTGTCGAG-3′ and reverse 5′-AGGAAGTGTGGGCTGAGGTAGA-3'.

2.10. RNA-sequencing (RNA-seq)

RNA-seq and bioinformatic analyses were performed by Beijing Genomics Institute (BGI). Sequencing and expression level of each gene was calculated by fragments per kilobase of exon per million reads mapped (FPKM). Based on the gene expression level, differentially expressed genes (DEGs) were identified between groups. Fold-change in gene expression between 2 samples was calculated by log2 FPKM ratio of 2 samples.

2.11. Western blot analyses

Whole-cell protein lysates were extracted with SDS protein lysis buffer with proteinase inhibitor (MedChemExpress) and protein concentration determined by standard Bradford protein assay (Bio-Rad) at 590 nm using the microplate reader (Labexim Products, University Research Facility in Life Sciences of The Hong Kong Polytechnic University). Twenty micrograms of protein were loaded onto SDS-PAGE gels and transferred onto PVDF membrane after electrophoresis. After 1 h blocking in 5% skim milk and incubation of primary antibody (1:2000) at 4 °C overnight, the membrane was incubated with secondary antibody (anti-rabbit or anti-mouse antibody, 1:2000) at room temperature for 1 h. The membrane was washed 3 times with 1X TBST at 5-min intervals before and after secondary antibody incubation. Clarity Western ECL Substrate (Bio-Rad) was used for detection. Primary antibody dilution ratios: Merlin (D1D8) rabbit mAb (Cell Signaling Technologies, CST), non-phospho (active) β-catenin (Ser33/37/Thr41) (D13A1) rabbit mAb (CST), β-catenin (D10A8) rabbit mAb (CST), MYC (CST) and β-actin mouse mAb (ABclonal). Semi-quantitative analyses of protein bands were done using ImageJ software. Intensity of bands was calculated as an arbitrary value relative to ACTB expression level.

2.12. Statistical analyses

Values are presented as mean ± standard deviation (SD). Statistical significance was assessed by two-tailed, unpaired Student's *t*-test with *P*-values (Prism Software). P values < 0.05 were considered as statistically significant.

3. Results

3.1. Exacerbated liver tumorigenicity by gRNA library in the context of $CTNNB1^{S33Y}$ overexpression

After successful hydrodynamic delivery of transposon vectors, both FSE mice injected with gRNAs together with $CTNNB1^{S33Y}$ and FS mice injected with $CTNNB1^{S33Y}$ alone developed tumor nodules (Fig. 1A and B). Using the number of tumor nodules observed as a measure of tumorigenicity, FSE mice injected with $CTNNB1^{S33Y}$/gRNA ($n = 8$) had significantly more tumor nodules ($P = 0.0161$, unpaired Student *t*-test) than FS animals injected with $CTNNB1^{S33Y}$ alone ($n = 5$) from 80- to 113-days post-hydrodynamic injection (Fig. 1C). There were also statistically significant differences in liver to whole body weight found between experimental $CTNNB1^{S33Y}$/gRNA and control $CTNNB1^{S33Y}$ groups ($P = 0.0333$, unpaired Student *t*-test; Fig. 1D). Representative liver tumor nodules and normal liver tissues, isolated from injected experimental $CTNNB1^{S33Y}$/gRNA FSE mice, were positive for the injected transgenes by RT-PCR (Fig. 1E). Subsequently, NGS on hepatic DNA isolated from tissue samples was used to identify the gRNAs and their corresponding target genes that would complement *CTNNB1*-assosicated HCC tumorigenesis. From 8 FSE mice (3 males and 5 females), a total of 105 liver tumor nodules and 67 adjacent normal tissues were isolated for NGS. In addition to the liver tumor nodules extracted for NGS, other histopathological phenotypes observed in the livers of experimental animals as shown in Supplementary Fig. 1. The FSE and FS mice used in this study as summarized in Table 1.

3.2. Identifying candidate target genes from the gRNA library

Genomic DNA from liver tumor nodules, together with adjacent macroscopically normal liver tissues, were extracted for NGS to

Table 1
FSE mice injected with $CTNNB1^{S33Y}$/gRNA.

	PHI	Liver to body (%)	No. of nodules
FSE F377	17	8.27	0
FSE F371	22	6.2	0
FSE F372	22	6.88	0
FSE F376	22	8.85	0
FSE M372	25	5.07	0
*FSE M351	65	10.9	19
*FSE F373	66	15.79	27
*FSE M561	69	14.25	30
FSE F351	80	14.86	36
*FSE F352	87	19.69	49
*FSE F461	89	18.2	36
*FSE F462	89	15.19	14
*FSE F581	97	15.06	17
*FSE M584	97	21.14	83
FSE M562	113	15.97	23
FS F1476	80	11.5	10
FS F1481	80	10	2
FS F1501	80	18.8	2
FS F1502	80	11.3	3
FS M1315	112	13	10

*Mice used for Illumina sequencing of gRNAs.
FS mice injected with $CTNNB1^{S33Y}$ only.

Table 2
Summary of the distribution and number of gRNAs sequenced in both tumor and normal samples.

	Tumor sample			Normal sample		
	<5%	5–10%	>10%	<5%	5–10%	>10%
No. of samples	18	19	68	42	17	8
No. of gRNAs sequenced	44617	21974	51183	64720	24023	9812
Average no. of gRNAs per sample	2478.72	1156.53	752.69	1540.95	1413.12	1226.5

<5%, samples with gRNA reads that are <5% of the total reads; 5–10%, samples with gRNA reads that are from 5 to 10% of the total reads; >10%, samples with gRNA reads that are >10% of the total reads.

identify the causative gRNA(s) that exacerbated liver tumorigenicity with *CTNNB1*^{S33Y}. From 105 tumor samples, a total of 33,951,863 gRNA reads were sequenced (average 323,351.08), while a total of 22,642,019 gRNA reads were sequenced from 67 normal samples (average 337,940.58). The distribution and number of gRNAs sequenced in samples as summarized in Table 2. The number of samples with dominant gRNAs (>5%) was significantly more in the tumor group than the normal samples (Fisher's exact test, $P < 0.00001$), suggesting that gRNA-mediated loss-of-function increased tumorigenicity. Using a 5% hit frequency rate criteria (sequencing count for a particular gRNA targeting its specific gene was at least 5% of the total sequencing counts in each sample), 206 genes were identified (Supplementary Data 2). The tissue distribution of these 206 genes were as follows: 30 and 162 genes were found exclusively in adjacent normal liver tissue and liver tumor nodules, respectively; while 14 genes were found to be overlapped between adjacent normal liver tissue and liver tumor nodules (Fig. 2A). Therefore, from the 206 genes identified in our *in vivo* screen, 19 candidate genes

A

Hit (%, T/N)	No. of hits (T/N)	Gene
19.05/11.94	20/8	*Max*
12.38/10.45	13/7	*Lingo3*
10.48/8.96	11/6	*Itsn1*
9.52/7.46	10/5	*Gpx1*
6.67/2.99	7/2	*Sav1*
5.71/1.49	6/1	*Atp6v0a1*
4.76/1.49	5/1	*Prcc*
0.95/2.99	1/2	*Glra3*
0.95/2.99	1/2	*Cux1*
0.95/2.99	1/2	*Gdnf*
0.95/2.99	1/2	*Flcn*
0.95/1.49	1/1	*Ednrb*
0.95/1.49	1/1	*Gjb1*
0.95/1.49	1/1	*Fgf3*

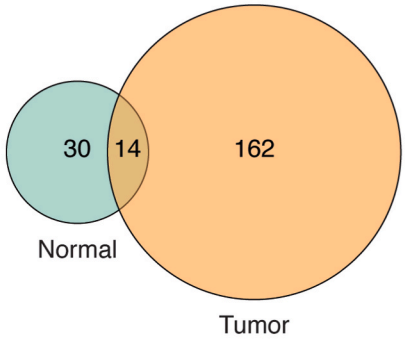

Hit (%)	No. of hits	Gene
6.67	7	*Nf2*
2.86	3	*Eif4g2*
2.86	3	*Midn*
2.86	3	*Ssh3*
2.86	3	*Tbx3*

B

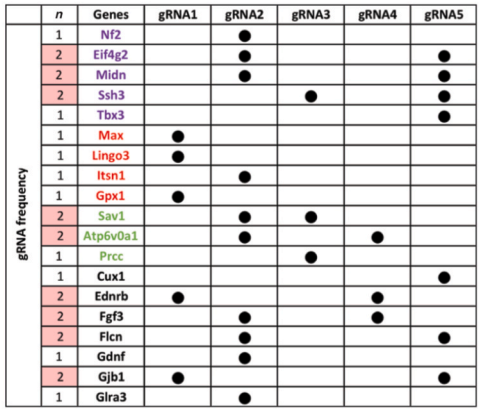

Fig. 2. Identifying the candidate genes targeted by the gRNA library in liver samples using next-generation sequencing. (**A**) Tissue distribution of 206 genes identified by gRNAs using a 5% hit frequency rate. The 14 overlapped candidate genes identified in both normal and tumor samples, number and percentage of gRNA hits in corresponding tissue samples as shown in the table (**right**). The top 5 candidate genes identified exclusively in tumor samples, number and percentage of gRNA hits as shown in the table (**left**). Hit, percentage of the number of hits in either tumor ($n = 105$) or normal ($n = 67$). (**B**) Summarized table showing the number of gRNAs that were sequenced from the tissue samples for the 19 candidate genes. Purple, moderate hits exclusively in tumor samples only; Red, high hits in both normal and tumor samples, Green, high hits in tumor but low hits in normal samples; Black, very low hits in both tumor and normal samples. *n*, frequency of gRNA identified from tumor and/or normal samples. (For interpretation of the references to colour in this figure legend, the reader is referred to the Web version of this article.)

(14 overlapped and top 5 genes from the tumor only samples) were short-listed based on their gRNA gene hit frequencies in either tumor and/or normal tissue samples (Fig. 2A). From the sequenced gRNAs targeting the 19 candidate genes, 53% of the genes were targeted by a single predominant gRNA while the remaining genes were targeted by two gRNAs (47%) (Fig. 2B). The targeted protein regions and domains of the candidate genes by their corresponding gRNAs as summarized in Table 3.

3.3. Clinical relevance of the candidate genes

The role and genetic alterations of the 19 candidate genes in human HCC were determined using the TCGA database

Table 3
Targeted protein regions of candidate genes by gRNAs.

gRNA targeting regions	Protein Region	Protein Sequence	Protein Domain
Nf2_CCDS24391.1_ex10_11:4806263-4806285:-_5-2	190-196	AWYAEHR	B41/FERM_M
Eif4g2_CCDS40087.1_ex9_7:111076996-111077018:-_5-2	352-359	EGPFMPPR	MIF4G
Eif4g2_CCDS40087.1_ex17_7:111080254-111080276:+_5-5	52-59	PARSTRRD	
Midn_CCDS24011.1_ex4_10:80153856-80153878:-_5-5	186-193	ALRVGDHM	-
Midn_CCDS24011.1_ex0_10:80150212-80150234:-_5-2	45-53	DLSVPHDET	UBQ
Ssh3_CCDS29425.1_ex12_19:4268531-4268553:+_5-5	33-36	LQRR-intron	SSH-N
Ssh3_CCDS29425.1_ex11_19:4267731-4267753:+_5-3	112-113	RPQDDIRL-intron	
Tbx3_CCDS19613.1_ex1_5:119674195-119674217:+_5-5	187-194	HPDSPATG	TBOX
Max_CCDS36479.1_ex0_12:76938744-76938766:-_5-1	90-94	Intron-VRALEKAR	LUCINE ZIPPER
Lingo3_CCDS24035.1_ex0_10:80835245-80835267:-_5-1	276-284	LSHNPISMV	LRR 9 (LUCINE RICH REPEAT)
Itsn1_CCDS37402.1_ex4_16:91801650-91801672:-_5-2	157-164	PLANGAPP	JUN-LIKE TRANSCRIPTION FACOTR
Gpx1_CCDS23522.1_ex0_9:108339458-108339480:-_5-1	49-56	TTIRDYTE	GSH_PEROXIDASE/ACTIVE RESIDUES
Sav1_CCDS25956.1_ex3_12:69984404-69984426:+_5-2	107-114	VPRECGSS	-
Sav1_CCDS25956.1_ex3_12:69984428-69984450:+_5-3	98-106	YLVRSLAD	-
Atp6v0a1_CCDS25443.1_ex5_11:101027288-101027310:-_5-2	177-183	RERIPTF	V_ATPase_I
Atp6v0a1_CCDS25443.1_ex6_11:101029172-101029194:-_5-4	212-217	intron-GDYVHK	
Prcc_CCDS17456.1_ex6_3:87884891-87884913:+_5-3	144-151	PVRIAAPE	-
Cux1_CCDS39328.1_ex21_5:136408009-136408031:+_5-5	59-65	DLRKQVA	-
Ednrb_CCDS27317.1_ex6_14:103843263-103843285:-_5-4	65-71	RSSAPAE	-
Ednrb_CCDS27317.1_ex6_14:103843047-103843069:-_5-1	137-141	NILIA	7tm_1
Fgf3_CCDS22051.1_ex1_7:144840672-144840694:+_5-4	75-81	ILEITAV	FGF
Fgf3_CCDS22051.1_ex0_7:144838817-144838839:+_5-2	37-44	EHLGGAPR	FGF
Flcn_CCDS24777.1_ex8_11:59802161-59802183:+_5-2	189-195	LLGRIRG	folliculin
Flcn_CCDS24777.1_ex9_11:59803857-59803879:+_5-5	89-96	AVGHPGYI	-
Gdnf_CCDS27371.1_ex1_15:7815744-7815766:-_5-2	74-79	FALTSD	-
Gjb1_CCDS30314.1_ex0_X:101384568-101384590:-_5-5	134-141	TYVISVVF	Connexin
Gjb1_CCDS30314.1_ex0_X:101384331-101384353:-_5-1	55-61	TLQPGCN	
Glra3_CCDS40340.1_ex1_8:55991120-55991142:+_5-2	41-46	LVATKE	LIC

Legend: Purple, moderate hits exclusively in tumor samples only; Red, high hits in both normal and tumor samples, Green, high hits in tumor but low hits in normal samples; Black, very low hits in both tumor and normal samples

(Supplementary Fig. 2A). From the 5 candidate genes identified exclusively in tumor samples, expression levels of 3 genes (*NF2*, *MIDN* and *SSH3*) displayed negative correlation with *CTNNB1* expression (Supplementary Fig. 2B). Two genes (*TBX3* and *EIF4G2*) displayed positive correlation with *CTNNB1* expression (Supplementary Fig. 2C). From the 14 candidate genes identified overlapping with both normal and tumor samples, expression levels of 5 genes (*MAX*, *GPX1*, *ATP6V0A1*, *PRCC* and *GJB1*) displayed negative correlation with *CTNNB1* expression – indicating tumor suppressor gene function (*data not shown*). Nine genes (*LINGO3*, *CUX1*, *GLRA3*, *ITSN1*, *FLCN*, *SAV1*, *GDNF*, *EDNRB* and *FGF3*) displayed positive correlation with *CTNNB1* expression (*data not shown*).

3.4. Validating the role of NF2 with CTNNB1 in HCC tumorigenesis

NF2 knockout clones were successfully generated in SNU449 and HHL7 cells by targeting the FERM domains using the CRISPR/Cas9 system. Sanger sequencing confirmed the presence of indels in all clones (Supplementary Fig. 3A). *NF2*-deficiency was confirmed in both targeted cell lines by both qPCR and Western blot analyses (Fig. 3A and B, respectively). In *NF2*-deficient HHL7 cells, the expression level of *CTNNB1* was non-significant to that of the scramble control while its downstream target *MYC* expression level was significantly increased ($P = 0.0011$) (Fig. 3A). Importantly, Western blot analyses demonstrated significantly increased levels of both active CTNNB1 and MYC levels in *NF2*-deficient HHL7 cells (Fig. 3B). The transcription levels of *CTNNB1* and *MYC*, were both significantly higher in *NF2*-deficient SNU449 cells when compared to scramble controls (Fig. 3A). This result was recapitulated using Western blot analyses, showing significantly increased CTNNB1 (both total and active) and MYC levels in *NF2*-deficient SNU449 cells (Fig. 3B).

3.5. RNA-seq analyses of NF2-deficient cell lines

In addition, RNA-seq was performed on *NF2*-deficient cell lines compared with their scrambled controls. For the HHL7 cell lines, a total of 869 DEGs were obtained from *NF2*-deficient (HHL7_N) and scramble control (HHL7_S) – 218 up-regulated and 651 down-regulated DEGs (Supplementary Fig. 3B). For the SNU449 cell lines, a total of 1523 DEGs were obtained from *NF2*-deficient (SNU449_N) and scramble control (SNU449_S) – 763 up-regulated and 760 down-regulated DEGs (Supplementary Fig. 3C). Interestingly, there were 247 DEGs overlapping between the two cell lines (Supplementary Fig. 3D and Supplementary Data 3). Further KEGG analyses of these 247 overlapping DEGs revealed different pathways (Supplementary Data 4). Interestingly, when non-biased cluster analysis was performed these 247 DEGs from *NF2*-deficient and scramble control cell lines, 5 genes were identified – VCAN, ENG, GJA5, AFF3 and NPAS2 (Supplementary Table 2).

KEGG pathway enrichment analyses for HHL7 *NF2*-deficient (HHL7_N) and HHL7 scramble control (HHL7_S) revealed greatest candidate gene numbers in MAPK signaling, cancer, human papillomavirus infection and PI3K-Akt signaling pathways (Supplementary Fig. 4A). While KEGG pathway enrichment analyses for SNU449 *NF2*-deficient (SNU449_N) and SNU449 scramble control (SNU449_S) revealed greatest candidate gene numbers in cancer, cytokine-cytokine receptor interaction, MAPK signaling, microRNAs in cancer and PI3K-Akt signal pathways (Supplementary Fig. 4B). As preliminary data, the expression levels of *ENG* was confirmed by qPCR to be significantly upregulated in all *NF2*-knockout clones for both cell lines when compared with scramble control (Supplementary Fig. 5).

4. Discussion

The CTNNB1 molecular subclass of HCC remains an important subject for clinical studies due to its high incidence (28%, TCGA $n = 360$). The majority of these patients display missense CTNNB1 mutations resulting in the formation of a putative driver gene. Using two powerful genome editing tools, we performed an *in vivo* forward genetic screen for *CTNNB1* cooperating genes. FSE mice injected with gRNAs together with $CTNNB1^{S33Y}$ had more observable tumor nodules than FS animals injected with $CTNNB1^{S33Y}$ alone, indicating the exacerbated liver tumorigenicity was the result of the introduced gRNA library that cooperated with the $CTNNB1^{S33Y}$ (Fig. 1B). Histopathological changes observed in the gRNA/*CTNNB1* injected mice such as lymphoid cell infiltration, enlarged nuclei and cytoplasmic clearing of hepatocytes (likely representing glycogen deposition) and the presence of histiocytes are non-specific. However, the clustered hepatocytes with atypical enlarged nuclei represent hallmarks of HCC tumorigenesis [44–47]. Using 105 liver tumor nodules and 67 adjacent normal tissues from 8 FSE mice (3 males and 5 females), NGS was performed on hepatic DNA isolated from tissue samples in order to identify the gRNAs and their corresponding target genes that would complement *CTNNB1*-assosicated HCC tumorigenesis. Using a 5% hit frequency rate criteria, gRNAs targeting 206 genes were identified (Supplementary Data 2). The tissue distribution of these 206 genes were as follows: 30 and 162 genes were found exclusively in adjacent normal liver tissue and liver tumor nodules, respectively; while 14 genes were found to be overlapped between adjacent normal liver tissue and liver tumor nodules (Fig. 2A). The overlapped genes indicate their possible role in cooperating with *CTNNB1* in early stages of HCC tumorigenesis, while the genes identified exclusively in tumor samples suggest their potential roles in the maintenance of the tumorigenic state.

As our forward genetic screen focuses on identifying novel loss-of-function genes in the context of *CTNNB1* activation, candidate genes with negative correlation with *CTNNB1* in TCGA liver cancer database suggests possible tumor suppressor gene function. From the 19 candidate genes, 8 genes (*NF2*, *MIDN*, *SSH3*, *MAX*, *GPX1*, *ATP6V0A1*, *PRCC* and *GJB1*) display negative correlation to CTNNB1 expression – indicating tumor suppressor gene function. However, the remaining 9 candidate genes that display positive correlation with *CTNNB1* could suggest either a dominant negative tumor suppressor gene or an intermediary role in which the candidate gene can indirectly regulate the WNT/CTNNB1 pathway in HCC tumorigenesis. Therefore, from the 19 candidate genes identified in our *in vivo*

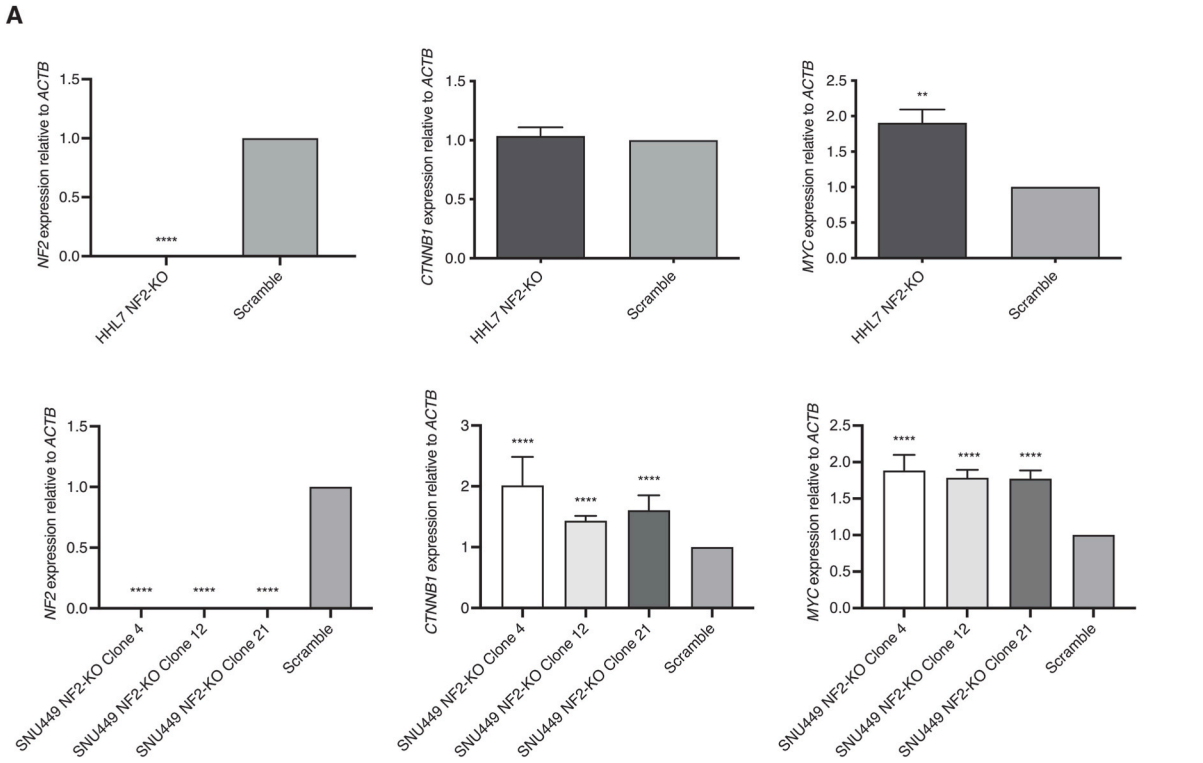

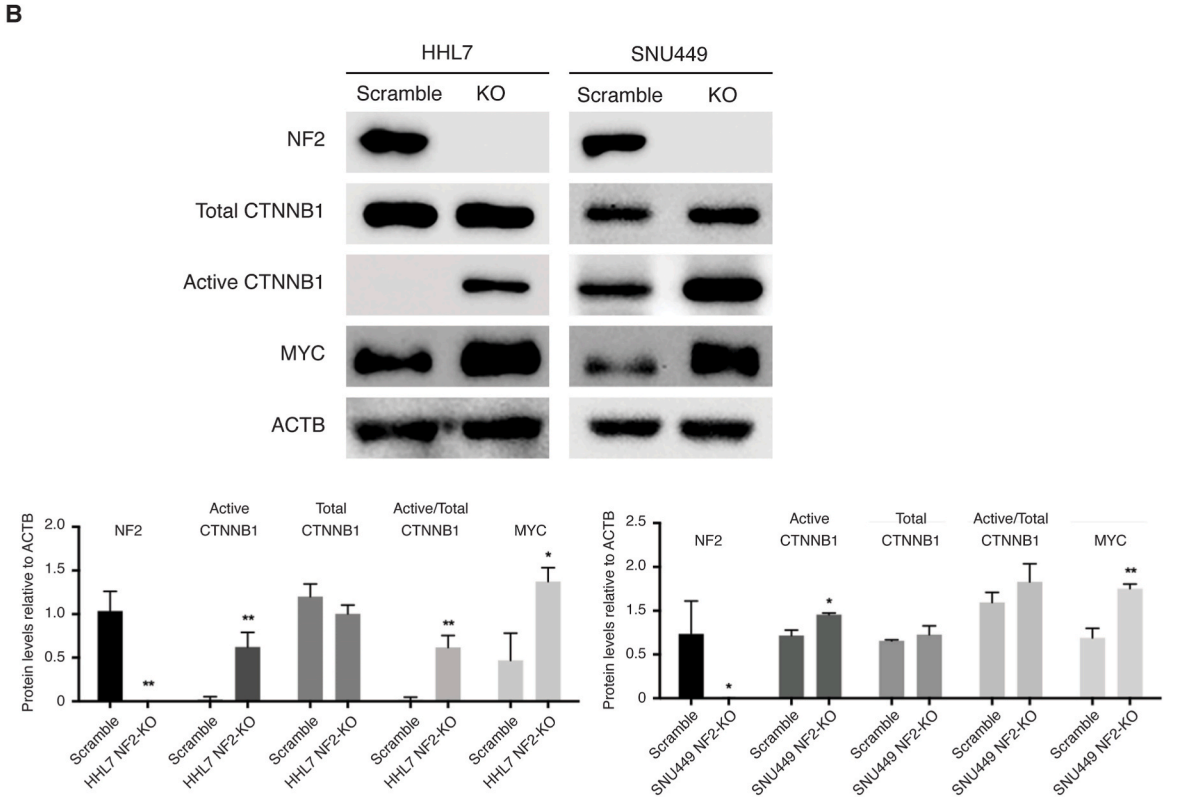

(caption on next page)

Fig. 3. Validating the role of *NF2* with *CTNNB1* in HCC tumorigenesis. (**A**) *NF2* knockout clones from both cell lines were confirmed by qPCR. In *NF2*-deficient HHL7 cells, expression level of *CTNNB1* was non-significant to that of the scramble control while its downstream target *MYC* expression level was significantly increased. Expression levels of both *CTNNB1* and *MYC*, were significantly higher in *NF2*-deficient SNU449 cells when compared to scramble controls. Expression levels of target genes were relative to *ACTB*, normalized with scramble and shown as mean ± SD. **, $P = 0.0011$; ****, $P < 0.0001$; two-tailed unpaired Student *t*-test. (**B**) Representative Western blots of *NF2* knockout clones from both cell lines. Protein levels of NF2, active CTNNB1, total CTNNB1 and MYC relative to ACTB. Representative semi-quantitative analyses of Western blot bands from *NF2* knockout clones of both cell lines. Protein levels of target genes were relative to ACTB and shown as mean ± SD. *, $P < 0.05$; **, $P < 0.01$; two-tailed unpaired Student *t*-test.

screen, neurofibromin 2 (*NF2*) gene, a known tumor suppressor gene with clinical relevance was validated in this proof-of-principle study (Fig. 2A). In previous *SB* transposon screens, *NF2* was identified as a candidate gene for osteosarcoma [48], while *SAV1* was identified in a NAFLD screen and its liver-specific deletion resulted in lipid accumulation, apoptosis and fibrogenesis [49]. While the *SB* system was used to overexpress *GDNF* as potential treatment for Parkinson's disease [50,51].

The interaction between *NF2* and *CTNNB1* in HCC tumorigenesis has not been fully elucidated. Dysregulation of *NF2* has been shown to drive HCC tumorigenesis via the Hippo/YAP signaling pathway by contributing to self-renewal, drug resistance and increased oncogenicity of the cancer cells [34,52,53]. A previous study has demonstrated a mutant form of *NF2*, lacking exons 2 to 4, could promote HCC tumorigenesis and promote metastatic events [54]. It has also been reported that the down-regulation of *NF2* in neurofibromatosis type 2 can promote WNT signaling by activating LPR6 receptor or Rac1 [24,55]. Similarly in pancreatic cancer and meningiomas, low levels of *NF2* can result in activated FOXM1/CTNNB1 activity, which in turn enhances WNT signaling [32,56]. Conversely, the suppression of WNT signaling pathway has been observed in normal *NF2* expressing breast cancer and pancreatic cancer cells [57]. As proof-of-principle validation, *NF2* gene expression was disrupted in two human liver cell lines using the CRISPR/Cas9 system. In corroboration with our forward genetic screen, *NF2* disruption resulted in upregulation of *CTNNB1* and its downstream target *MYC*.

Both MAPK and PI3K/AKT signaling pathways are regulated by WNT/CTNNB1 signaling during HCC tumorigenesis [58]. Using BioGRID analyses, we identified 269 non-redundant binding targets of NF2 protein. By comparing these non-redundant targets with known proteins in the WNT signaling pathway using KEGG, 16 candidate proteins were identified as possible interacting targets with NF2 in the WNT signaling pathway - AKT1, ARAF, CDK4, CDK6, EGFR, HGF, HRAS, IGF1R, KRAS, MET, MYC, NRAS, PRKCA, RAF1, SMAD3 and TP53. Interestingly, *SMAD3* is the only candidate protein also known to be involved in the Hippo signaling pathway. The interaction of SMAD3 with NF2 was identified using affinity capture-mass spectrometry [59].

Using RNA-seq data, non-biased cluster analysis of 247 DEGs from *NF2*-deficient and scramble control cell lines identified 5 genes (VCAN, ENG, GJA5, AFF3 and NPAS2) with possible mechanistic correlation with NF2 (Supplementary Table 2). Interestingly, the *ENG* expression was significantly upregulated in all *NF2*-knockout clones for both cell lines when compared with scramble control (Supplementary Fig. 5). ENG or CD105, is a homodimeric receptor located in the cellular membrane with several functions – such as the regulation of cell proliferation, cell migration and angiogenesis via the transforming growth factor beta pathway [60,61]. ENG serum levels are usually increased in HCC patients, making it a biomarker for HCC tumorigenesis [62–64]. It is hypothesized that the lack of functional *NF2* could increase WNT signaling activity by upregulating *ENG*. However, more investigation is required to validate this mechanistic association.

Taken together, the combination of the *SB* transposon and the CRISPR/Cas9 systems allows for a powerful genome wide loss-of-function screen to discover genes and pathways that drive HCC tumorigenesis. In the current study, stable integration of transposon plasmids carrying pools of gRNAs while overexpressing a mutant version of *CTNNB1* was achieved in the hepatocyte genome. The *Fah*-deficient model allows for hepatocytes to have a selective growth advantage as a result of the introduced transgenes (namely *CTNNB1* and gRNAs) that will proliferate and result in tumorigenesis, in the context of WNT signaling activation. In this proof-of-principle study, *NF2* was validated to have novel genetic association with *CTNNB1* in HCC tumorigenesis.

Declarations

Author contribution statement

Vincent W. Keng: Conceived and designed the experiments; Analyzed and interpreted the data; Wrote the paper.

Amy P. Chiu; Jeffrey C. To; Xiao-xiao Li: Performed the experiments; Analyzed and interpreted the data.

Michael A. Linden; Khalid Amin: Analyzed and interpreted the data.

Branden S. Moriarity: Contributed reagents, materials, analysis tools or data.

Kosuke Yusa: Conceived and designed the experiments; Analyzed and interpreted the data; Contributed reagents, materials, analysis tools or data.

Data availability statement

Data included in article/supp. material/referenced in article.

Declaration of competing interest

The authors declare that they have no known competing financial interests or personal relationships that could have appeared to influence the work reported in this paper

Acknowledgments

We would like to thank the Centralised Animal Facility (CAF), The Hong Kong Polytechnic University, for their excellent technical assistance with experimental animals described in this study. We would like to thank Ms Cynthia Chiu for her technical assistance in generating the NF2 knockout cell lines and performing the validation experiments; and Prof David A. Largaespada for the critical review of the manuscript.

V.W.K. was supported by Project 82073134 of the National Natural Science Foundation of China; State Key Laboratory of Chemical Biology and Drug Discovery (1-BBX8) and The Hong Kong Polytechnic University/UGC internal funding (1-ZVST); Research Impact Fund (PolyU R5050-18) from the Research Grant Council, Hong Kong Government.

K.Y. was supported by Wellcome Trust (WT206194).

V.W.K. and K.Y. were both supported by the Cooperative Research Program - Joint Usage/Research Center Program of Institute for Frontier Life and Medical Sciences, Kyoto University.

Appendix A. Supplementary data

Supplementary data to this article can be found online at https://doi.org/10.1016/j.heliyon.2023.e18774.

References

[1] J. Ferlay, et al., Estimates of worldwide burden of cancer in 2008: GLOBOCAN 2008, Int. J. Cancer 127 (12) (2010) 2893–2917.
[2] J.M. Llovet, A. Burroughs, J. Bruix, Hepatocellular carcinoma, Lancet 362 (9399) (2003) 1907–1917.
[3] P.A. Farazi, R.A. DePinho, Hepatocellular carcinoma pathogenesis: from genes to environment, Nat. Rev. Cancer 6 (9) (2006) 674–687.
[4] W.E. Naugler, et al., Gender disparity in liver cancer due to sex differences in MyD88-dependent IL-6 production, Science 317 (5834) (2007) 121–124.
[5] V.W. Keng, et al., Sex bias occurrence of hepatocellular carcinoma in Poly7 molecular subclass is associated with EGFR, Hepatology 57 (1) (2013) 120–130.
[6] Z. Li, et al., Foxa1 and foxa2 are essential for sexual dimorphism in liver cancer, Cell 148 (1–2) (2012) 72–83.
[7] D.Y. Chiang, et al., Focal gains of VEGFA and molecular classification of hepatocellular carcinoma, Cancer Res. 68 (16) (2008) 6779–6788.
[8] Y. Hoshida, et al., Integrative transcriptome analysis reveals common molecular subclasses of human hepatocellular carcinoma, Cancer Res. 69 (18) (2009) 7385–7392.
[9] S.P. Hussain, et al., TP53 mutations and hepatocellular carcinoma: insights into the etiology and pathogenesis of liver cancer, Oncogene 26 (15) (2007) 2166–2176.
[10] Y. Horie, et al., Hepatocyte-specific Pten deficiency results in steatohepatitis and hepatocellular carcinomas, J. Clin. Invest. 113 (12) (2004) 1774–1783.
[11] A.J. Dupuy, et al., A modified sleeping beauty transposon system that can be used to model a wide variety of human cancers in mice, Cancer Res. 69 (20) (2009) 8150–8156.
[12] V.W. Keng, et al., A conditional transposon-based insertional mutagenesis screen for genes associated with mouse hepatocellular carcinoma, Nat. Biotechnol. 27 (3) (2009) 264–274.
[13] K.A. O'Donnell, et al., A Sleeping Beauty mutagenesis screen reveals a tumor suppressor role for Ncoa2/Src-2 in liver cancer, Proc. Natl. Acad. Sci. U. S. A. 109 (21) (2012) E1377–E1386.
[14] J.D. Riordan, et al., Identification of rtl1, a retrotransposon-derived imprinted gene, as a novel driver of hepatocarcinogenesis, PLoS Genet. 9 (4) (2013), e1003441.
[15] E.A. Bard-Chapeau, et al., Transposon mutagenesis identifies genes driving hepatocellular carcinoma in a chronic hepatitis B mouse model, Nat. Genet. 46 (1) (2014) 24–32.
[16] J.D. Riordan, et al., Chronic liver injury alters driver mutation profiles in hepatocellular carcinoma in mice, Hepatology 67 (3) (2018) 924–939.
[17] B.R. Tschida, et al., Sleeping beauty insertional mutagenesis in mice identifies drivers of steatosis-associated hepatic tumors, Cancer Res. 77 (23) (2017) 6576–6588.
[18] H. Koike-Yusa, et al., Genome-wide recessive genetic screening in mammalian cells with a lentiviral CRISPR-guide RNA library, Nat. Biotechnol. 32 (3) (2014) 267–273.
[19] H. Wang, et al., One-step generation of mice carrying mutations in multiple genes by CRISPR/Cas-mediated genome engineering, Cell 153 (4) (2013) 910–918.
[20] P. Mali, et al., RNA-guided human genome engineering via Cas9, Science 339 (6121) (2013) 823–826.
[21] L. Cong, et al., Multiplex genome engineering using CRISPR/Cas systems, Science 339 (6121) (2013) 819–823.
[22] S.W. Cho, et al., Targeted genome engineering in human cells with the Cas9 RNA-guided endonuclease, Nat. Biotechnol. 31 (3) (2013) 230–232.
[23] H. Yin, et al., Genome editing with Cas9 in adult mice corrects a disease mutation and phenotype, Nat. Biotechnol. 32 (6) (2014) 551–553.
[24] E.E. Bosco, et al., NF2-deficient cells depend on the Rac1-canonical Wnt signaling pathway to promote the loss of contact inhibition of proliferation, Oncogene 29 (17) (2010) 2540–2549.
[25] L.V. de Assis, J. Locatelli, M.C. Isoldi, The role of key genes and pathways involved in the tumorigenesis of Malignant Mesothelioma, Biochim. Biophys. Acta 1845 (2) (2014) 232–247.
[26] N. Kumari, S. Saxena, U. Agrawal, Exosomal protein interactors as emerging therapeutic targets in urothelial bladder cancer, J. Egypt. Natl. Cancer Inst. 27 (2) (2015) 51–58.
[27] M. de Oliveira Taveira, et al., Genomic characteristics of trastuzumab-resistant Her2-positive metastatic breast cancer, J. Cancer Res. Clin. Oncol. 143 (7) (2017) 1255–1262.
[28] X. Zhu, et al., Moesin is a glioma progression marker that induces proliferation and Wnt/β-catenin pathway activation via interaction with CD44, Cancer Res. 73 (3) (2013) 1142–1155.
[29] K.H. Saba, et al., Loss of NF2 defines a genetic subgroup of non-FOS-rearranged osteoblastoma, J. Pathol. Clin. Res. 6 (4) (2020) 231–237.
[30] J.W. Kunstman, et al., Characterization of the mutational landscape of anaplastic thyroid cancer via whole-exome sequencing, Hum. Mol. Genet. 24 (8) (2015) 2318–2329.

[31] C. Kassab, et al., Genetic and immune profiling for potential therapeutic targets in adult human craniopharyngioma, Clin. Oncol. Res. 2 (3) (2019) 2–8.
[32] M. Quan, et al., Merlin/NF2 suppresses pancreatic tumor growth and metastasis by attenuating the FOXM1-mediated Wnt/β-catenin signaling, Cancer Res. 75 (22) (2015) 4778–4789.
[33] J. Hyun, et al., Dysregulation of the ESRP2-NF2-YAP/TAZ axis promotes hepatobiliary carcinogenesis in non-alcoholic fatty liver disease, J. Hepatol. 75 (3) (2021) 623–633.
[34] N. Zhang, et al., Molecular alterations of the NF2 gene in hepatocellular carcinoma and intrahepatic cholangiocarcinoma, Oncol. Rep. 38 (6) (2017) 3650–3658.
[35] K. Tzelepis, et al., A CRISPR dropout screen identifies genetic vulnerabilities and therapeutic targets in acute myeloid Leukemia, Cell Rep. 17 (4) (2016) 1193–1205.
[36] M. Grompe, et al., Loss of fumarylacetoacetate hydrolase is responsible for the neonatal hepatic-dysfunction phenotype of lethal albino mice, Gene Dev. 7 (12a) (1993) 2298–2307.
[37] V.W. Keng, et al., Modeling hepatitis B virus X-induced hepatocellular carcinoma in mice with the Sleeping Beauty transposon system, Hepatology 53 (3) (2011) 781–790.
[38] K.J. Wangensteen, et al., A facile method for somatic, lifelong manipulation of multiple genes in the mouse liver, Hepatology 47 (5) (2008) 1714–1724.
[39] V.W. Keng, et al., A conditional transposon-based insertional mutagenesis screen for genes associated with mouse hepatocellular carcinoma, Nat. Biotechnol. 27 (3) (2009) 264–274.
[40] V.W. Keng, et al., Sex bias occurrence of hepatocellular carcinoma in Poly7 molecular subclass is associated with EGFR, Hepatology 57 (1) (2013) 120–130.
[41] Keng V.W., Largaespada D.A., Villanueva A., Why men are at higher risk for hepatocellular carcinoma?, J. Hepatol. 57 (2012) 453-454.
[42] R.F. Clayton, et al., Liver cell lines for the study of hepatocyte functions and immunological response, Liver Int. 25 (2) (2005) 389–402.
[43] F.A. Ran, et al., Genome engineering using the CRISPR-Cas9 system, Nat. Protoc. 8 (11) (2013) 2281–2308.
[44] A. Zimmermann, Steatotic and Steatohepatitic Hepatocellular Carcinomas and Related Neoplasms, Springer International Publishing, Cham, 2016, pp. 229–250.
[45] E.M. Brunt, Histopathologic features of hepatocellular carcinoma, Clin. Liver Dis. (Hoboken) 1 (6) (2012) 194–199.
[46] M. Schlageter, et al., Histopathology of hepatocellular carcinoma, World J. Gastroenterol. 20 (43) (2014) 15955–15964.
[47] Q. Su, P. Bannasch, Relevance of hepatic preneoplasia for human hepatocarcinogenesis, Toxicol. Pathol. 31 (1) (2003) 126–133.
[48] N.A. Temiz, et al., RNA sequencing of Sleeping Beauty transposon-induced tumors detects transposon-RNA fusions in forward genetic cancer screens, Genome Res. 26 (1) (2016) 119–129.
[49] T. Kodama, et al., Molecular profiling of nonalcoholic fatty liver disease-associated hepatocellular carcinoma using SB transposon mutagenesis, Proc. Natl. Acad. Sci. U. S. A. 115 (44) (2018), E10417-E10426.
[50] L. Stahn, et al., Sleeping Beauty transposon system for GDNF overexpression of entrapped stem cells in fibrin hydrogel in a rat model of Parkinson's disease, Drug Deliv. Transl. Res. 13 (6) (2023) 1745–1765.
[51] J. Rasinska, et al., Transposon-mediated glial cell line-derived neurotrophic factor overexpression in human adipose tissue-derived mesenchymal stromal cells: a potential approach for neuroregenerative medicine? J. Tissue Eng. Regen. Med. 16 (6) (2022) 515–529.
[52] V. Valero 3rd, T.M. Pawlik, R.A. Anders, Emerging role of Hpo signaling and YAP in hepatocellular carcinoma, J. Hepatocell. Carcinoma 2 (2015) 69–78.
[53] T. Wang, et al., Epigenetic restriction of Hippo signaling by MORC2 underlies stemness of hepatocellular carcinoma cells, Cell Death Differ. 25 (12) (2018) 2086–2100.
[54] Z.L. Luo, et al., A splicing variant of Merlin promotes metastasis in hepatocellular carcinoma, Nat. Commun. 6 (2015) 8457.
[55] S. Kim, E.H. Jho, Merlin, a regulator of Hippo signaling, regulates Wnt/β-catenin signaling, BMB Rep. 49 (7) (2016) 357–358.
[56] J. Deng, et al., The CREB-binding protein inhibitor ICG-001: a promising therapeutic strategy in sporadic meningioma with NF2 mutations, Neurooncol. Adv. 2 (1) (2020) vdz055.
[57] K.A. Morrow, et al., Loss of tumor suppressor Merlin results in aberrant activation of Wnt/β-catenin signaling in cancer, Oncotarget 7 (14) (2016) 17991–18005.
[58] X.H. Wang, et al., Wnt/beta-catenin signaling regulates MAPK and Akt1 expression and growth of hepatocellular carcinoma cells, Neoplasma 58 (3) (2011) 239–244.
[59] L. Zhou, et al., The scaffold protein KSR1, a novel therapeutic target for the treatment of Merlin-deficient tumors, Oncogene 35 (26) (2016) 3443–3453.
[60] M.J.A. Schoonderwoerd, M.-J.T.H. Goumans, L.J.A.C. Hawinkels, Endoglin: beyond the endothelium, Biomolecules 10 (2) (2020) 289.
[61] K.-S. Jeng, et al., The role of endoglin in hepatocellular carcinoma, Int. J. Mol. Sci. 22 (6) (2021) 3208.
[62] D. Yu, et al., Particular distribution and expression pattern of endoglin (CD105) in the liver of patients with hepatocellular carcinoma, BMC Cancer 7 (1) (2007) 122.
[63] E. Yagmur, et al., Elevation of endoglin (CD105) concentrations in serum of patients with liver cirrhosis and carcinoma, Eur. J. Gastroenterol. Hepatol. 19 (9) (2007) 755–761.
[64] S. Teama, et al., Increased serum endoglin and transforming growth factor β1 mRNA expression and risk of hepatocellular carcinoma in cirrhotic Egyptian patients, Asian Pac. J. Cancer Prev. APJCP 17 (5) (2016) 2429–2434.